Data-Driven System Identification Modelling for Multi-Float M4 Wave Energy Converter with Elastic Bed-Buoy-Bow Float Mooring

Xuefei Wang, Danni Liang, Mengxiao Li, Peter Stansby and Long Zhang

Abstract—**This paper makes a unique contribution to apply data-driven system identification methods to model the mooring of 6-float M4 wave energy converter (WEC). Within the M4 system, elastic mooring cables connect the buoy to the basin bed, and the inelastic lines link the buoy to the bow float. Two linear models including autoregressive with exogenous inputs (ARX) model and the Box-Jenkins (BJ) model are used to identify the systems between three typical features: the wave surface elevation, the mooring force in the elastics, and the motions of the bow float. The bow float motions include pitch, surge and heave. The performance of identified models are determined from wave basin experiments under a number of different wave conditions in terms of significant wave heights and peak wave periods. Different sampling rate and model orders are also tested during identification. It is found that for both ARX and BJ models, low orders and sampling rate are sufficient to identify the M4 WEC systems.**

Index Terms—**System Identification, M4 Wave Energy Converter, Mooring Configuration**

I. Introduction

WITH the expanding global energy demand, the inadequate reserves of fossil fuels, the energy crisis is severer than ever before [1]. In order to alleviate the severity of the energy crisis, renewable energy needs to be exploited and put into use urgently [2]. As one of the renewable energy resources, the ocean contains a vast volume of wave energy, tidal energy, ocean current energy and salinity gradient energy. Among these, wave energy has the potential to be one of the major electricity generation resources in the long term, since a substantial amount of studies show that ocean wave has average potential power just slightly less than natural wind [3]. For example, Ireland announces that the wave energy will occupy approximately 40% of the overall electricity generated from renewable resources by 2050 [4]. In Australia, wave energy production from west sea coast will achieve 35% of the capacity installed from wind power by next decade [5]. However, unlike the wind power that has been widely used in a large industrial scale, the wave power has not been extensively deployed in real applications yet [6]. The industrial-scale implementation of wave energy is still at an early stage and requires deeper research and development [7].

A wave energy converter (WEC) transforms the kinetic energy of ocean wave into electricity. Currently, there exists several different wave energy conversion technologies being researched and developed worldwide, such as oscillating bodies, oscillating water columns, and over-topping modules [8–10]. In this paper, a 6-float wave energy converter M4 is used for modelling, which is developed by the University of Manchester. Fig.1 shows the 6 degree of freedom M4 WEC which includes a bow float, three mid floats and two stern floats with beams hinged above the outer mid floats [11]. The wave forces of each individual float are subject to pitch, surge and heave motions. The M4 WEC naturally heads towards the wave direction by drift forces. Fig.2 shows the mooring to the bow float which consists of an elastic cable, with stiffness of about 100N/m for tension greater than 15N, see Fig.7 in [12], from the bed to a spherical buoy and an inelastic cable from the buoy to the bow float.

The M4 WEC has been well modelled numerically to evaluate the M4 performance and further enhance the device design and upgrade iteratively [13]. However, numerical modelling of M4 WEC mooring forces in steep waves has the following limitations which may have impacts on the system design and manufacture.

1) While linear diffraction/radiation modelling gives good predictions of response and power in operational and surprisingly also of motion in extreme conditions, mooring forces are highly nonlinear and are not well predicted [11].
2) Computational fluid dynamics (CFD) modelling requires massive computations to precisely model the physical wave-structure interaction of the WEC, which may take hours even days to complete the modelling process. Especially for WEC system useful lifetime estimation purpose, the modelling procedure requires to be conducted repeatedly to cover a long period of the fatigue life cycle [14].
3) There generally exists mismatch between the numerical model and the M4 WEC system for

This work was supported by the U.K. Engineering and Physical Sciences Research Council (EPSRC) and Royal Society under Grant EP/V039946/1. Support for Lir ocean basin access through the EU Marinet2 programme, project M4moor (reference number 5031), is also gratefully acknowledged. (Corresponding author: Long Zhang)

X. Wang, D. Liang, M. Li, P. Stansby and L. Zhang are with the School of Engineering, The University of Manchester, Manchester, M13 9PL, U.K. (e-mail: xuefei.wang@manchester.ac.uk, p.k.stansby@manchester.ac.uk, long.zhang@manchester.ac.uk).

Digital Object Identifier 10.36688/ewtec-2023-513

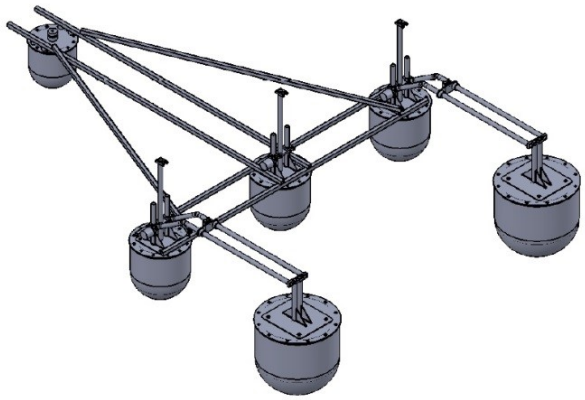

Fig. 1 Isometric view of 6-float M4 WEC system

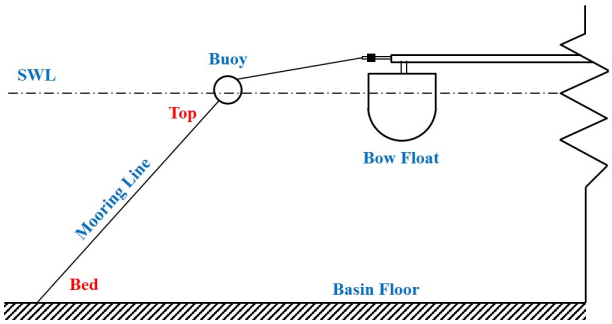

Fig. 2 Mooring configuration of the physical experiment showing the buoy and bow float

mooring forces. The modelling accuracy may be limited to a certain degree due to the selection of modelling methods and a constrained range of features [12]. This discrepancy may reduce the confidence level of system design.

Given these limitations, this paper aims to use system identification methods to determine the models between the waves and the mooring of M4 WEC system. Compared with numerical modelling, system identification methods enjoys the following advantages:

1) System identification is a data-driven method, which uses real-time measurement signals and can be adopted for online applications [15]. In some cases, even limited measurement datasets may produce useful information of the unknown system parameters, and there is no need to have prior knowledge of the status of the M4 WEC system parameters.
2) System identification methods require less computations and significantly reduce the modelling time [16]. This simplicity speeds up the modelling when it is conducted repeatedly and routinely for a M4 WEC mooring fatigue lifespan prediction purpose.
3) The design of the M4 WEC mooring system can be advised based on both the numerical models and the identified models. This may provide a more comprehensive understanding of the WEC system and deliver a better design strategy for further manufacturing. The combined consideration is likely to reduce the mismatch between the model and the system to a minimum. The high confidence level of design enables to enhance the wave energy production.

The modelling focuses on the model between the surface elevation of waves and the motions of the bow float of M4 under different wave conditions, and the model between the wave surface elevation and the mooring forces in the elastic cables connected from the basin bed to the buoy. The main contributions of this paper are summarized as follows:

1) This paper aims to use data-driven system identification methods to model the multi-float M4 WEC device in terms of the wave surface elevation, the mooring forces (top force and bed force) and the bow float motions (heave, pitch and surge). The dampers for power absorption at the hinges are disengaged for these tests which are mainly concerned with survivability in extreme conditions [12].
2) The data was collected from M4 WEC water basin experiments which covers a wide range of major WEC operating conditions including 7 cases in terms of different wave height and peak period [12]. This provides sufficient flexibility to test the modelling and shows high level of confidence in modelling accuracy.
3) Two different linear model types (ARX and BJ) are used to model the M4 WEC converter considering the impacts of both model complexity and sampling rate. M4 WEC modelling results are compared using selected criteria including fitting, FPE and MSE values.

The rest of this paper is organized as follows: Section II introduces the system identification modelling methods including both linear and nonlinear models. Section III introduces the M4 WEC data acquisition experimental data. Section IV shows the experiments setup, procedures, results analysis and validations. Section V concludes the paper.

II. Linear ARX and BJ system identification

The 6-float M4 WEC has a complex nonlinear mooring system, however, to enjoy the acceptable model accuracy, the system can be approximated as a series of piecewise linear models around different operating conditions. In this paper, the linear ARX and BJ models are used, and a brief theoretical background of these two models is provided in this session.

As the input and output data are sampled in the discrete time domain, discrete-time ARX and BJ models are used here. The mathematical formulation of ARX model is given by [15]:

$$a(z)y_k = b(z)u_k + e_k \tag{1}$$

where

$$\begin{aligned} a(z) &= 1 + a_1 z^{-1} + a_2 z^{-2} + \ldots + a_n z^{-n} \\ b(z) &= 1 + b_1 z^{-1} + b_2 z^{-2} + \ldots + b_m z^{-m} \end{aligned} \tag{2}$$

and $k = 1, ..., N$. N stands for the total number of samples, z^{-1} is the delay operator, namely, $y(t-1) = z^{-1}y(t)$. u_k, y_k and e_k represent the input, output and

error at time interval k, respectively. $a(z)$ and $b(z)$ are the model coefficient vectors for the output y_k and input u_k with orders n and m. The error e_k is assumed as a white noise in this case.

Denote φ_k and θ as the regressor vector and the parameter vector respectively:

$$\varphi_k = [-y_{k-1} \ \cdots \ -y_{k-n} \ u_{k-1} \ \cdots \ u_{k-m}] \tag{3}$$

$$\theta = [a_1 \ \cdots \ a_n \ b_1 \ \cdots \ b_m]^T \tag{4}$$

According to the definition in equation (3) and (4), equation (1) can be expressed as

$$y_k = \widehat{y}_k + e_k \tag{5}$$

where the prediction estimate of y_k is denoted as $\widehat{y_k} = \varphi_k\theta$. It is assumed that the error e_k has identical Gaussian distribution. To minimize that error, a cost function is defined by

$$J(\theta) = \sum_{k=n+1}^{N} e_k^2 = \sum_{k=n+1}^{N} \left(y_k - \widehat{y_k}(\theta)\right)^2 \tag{6}$$

The optimal selection of the system parameter $\hat{\theta}$ is derived by

$$\hat{\theta} = \arg\min_{\theta} J(\theta) \tag{7}$$

As a similar but more complex structure, BJ model has four polynomials (h, f, c, d) and can be described as [17]

$$y_k = \frac{h(z)}{f(z)}u_k + \frac{c(z)}{d(z)}e_k \tag{8}$$

where

$$\begin{aligned} h(z) &= 1 + h_1 z^{-1} + h_2 z^{-2} + \ldots + h_n z^{-\lambda_h} \\ f(z) &= 1 + f_1 z^{-1} + f_2 z^{-2} + \ldots + f_n z^{-\lambda_f} \\ c(z) &= 1 + c_1 z^{-1} + c_2 z^{-2} + \ldots + c_n z^{-\lambda_c} \\ d(z) &= 1 + d_1 z^{-1} + d_2 z^{-2} + \ldots + d_m z^{-\lambda_d} \end{aligned} \tag{9}$$

These four coefficient vectors $h(z)$, $f(z)$, $c(z)$ and $d(z)$ offer the BJ model more flexible and complicated description of the model structure, with λ_h, λ_f, λ_c and λ_d model orders respectively. Obviously, the ARX model is a special case of BJ model structure by setting $f(z) = a(z)$, $c(z) = 1$ and $d(z) = a(z)$. Similar as equation (7), the optimal parameter selection of BJ model is given by

$$\hat{\theta}' = \arg\min_{\theta'} J(\theta', y_k, u_k) \tag{10}$$

where

$$J(\theta', y_k, u_k) = \sum_{k=1}^{N} e_k^2 \tag{11}$$

In this paper, three criteria are chosen to evaluate the performances of the identified model candidates including mean square error (MSE), Akaike's final prediction error (FPE) and fitting percentage. MSE (e_m) is defined as [18]:

$$e_m = \frac{1}{N}\sum_{k=1}^{N} (y_k - \hat{y}_k)^2 \tag{12}$$

where y_k is the measured output, $\hat{y}_k$ is the predicted output. If e_m is equal to or close to 0, it means the measured outputs match the predicted one. A large value of e_m indicates the large error between the model and the system.

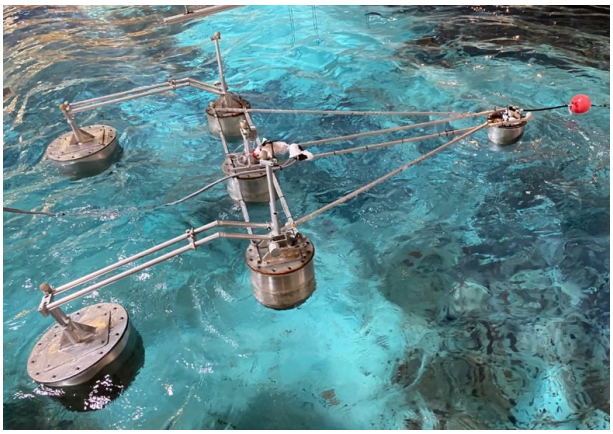

Fig. 3 Aerial photo of WEC with mooring in the wave basin

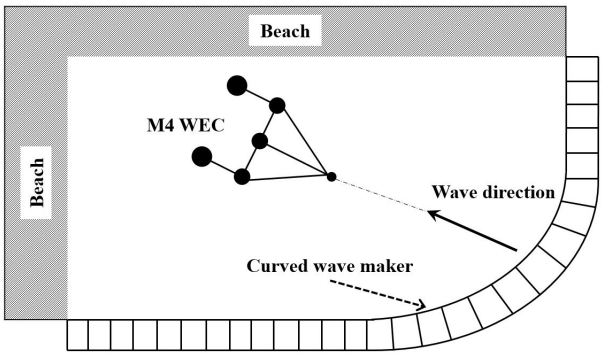

Fig. 4 Lir Ocean Basin of University College Cork, showing wavemakers, beach and M4 WEC

FPE (e_f) is described as [18]:

$$e_f = \left(\frac{N+p+1}{N-p-1}\right)\hat{\sigma}_p^2 \tag{13}$$

Where p is the order of the model and $\hat{\sigma}_p$ is the estimation of the prediction error power when the order is p. When FPE is minimised, the order of the system can be selected. Similar as MSE, the smaller value of e_f indicates that the identified model better describes the WEC system.

III. Experiments Set-up and Data Selection

The experiments were carried out in the Lir Ocean Basin of University College Cork, Ireland. An aerial photo of the experiment configuration is shown in Fig.3, and Fig.4 shows in detail that the basin has a curved line of 80 wave makers with sloping beaches on the two sides. The wave surface elevations, the mooring forces and the motions of the bow float are recorded during the tests.

This work selects three representative data sets for analysis, which are sea surface elevation, mooring force (top and bed force) and motions (pitch, surge and heave). In this paper, three different types of single-input single-output models are constructed. The first one is to model the dynamics between surface elevation and motions where the elevation is the model input and motion is the model output. The second one

TABLE I Three system identification schemes

Model Scheme	Model Input	Model Output
A	Elevation	Motion
B	Force	Motion
C	Elevation	Force

TABLE II Different significant wave heights and mean wave periods

Case	H_s/m	T_p/s
1	0.06	1.0
2	0.06	1.2
3	0.06	1.4
4	0.06	1.8
5	0.13	1.2
6	0.16	1.4
7	0.16	1.8

uses mooring force as the input and motion as output. In the third model, elevation is the input and mooring force is the output. Table I summarizes these three models. As shown in Fig.2, the surface elevation is measured with no WEC in the basin, and the mooring force is the force of the cable moored to the bed with top force measuring the force near buoy and bed force measuring the mooring force near the basin floor. The experiments are conducted in seven cases in terms of different significant wave heights (0.06m, 0.13m, 0.16m) and mean wave periods (1.0s, 1.2s, 1.4s, 1.8s), and they are briefly summarized in Table II.

The acquisition of raw data is completed within the experimental time of 600s. The sampling frequency for each measured variable is different and produces different number of samples. The surface elevation has 76800 samples with a sampling frequency of 128Hz. The mooring force has 30000 samples with a sampling frequency of 50Hz. The surge motion has 19200 samples with a sampling frequency of 32Hz. For the system identification, the sampling rate for both input and output measurements has to be the same. The sampling rate of the surface elevation is around 140Hz while the rate for motion is 32Hz which means that the sampling rate of surface elevation is 4 times faster than the motions. For the modelling, the sampling rate of surface elevation should be the same as the motion data. In this work, as a result, the collected data are re-sampled to make sure the input and output data have the same sampling rate. Fig. 5 shows the time domain plots of the three re-sampled measurements over time.

Take the surface elevation and mooring force as a group of data, the former is the input data and the latter is the output data. Similarly, for mooring force and surge motion data, the former is input data and the latter is output data. The data volume of the three data is different. The other two data are sampled at equal intervals. In the end, the data volume of the three data is the same as 19200. Original data can be divided into training and validating data. The waves are generated by the wave-making device. During the initial period of the experiment, the waves are not fully developed. Hence, to validate the measurements, the samples before 2200 are removed and the rest of samples are used for modelling. Therefore, multi-step prediction is required. In this work, three and five prediction steps are selected to compare with one prediction step modelling.

IV. Modelling Results Analysis

In this session, three different types of models with different input-output pairs are constructed under different modelling settings. Results from theses three models are given one by one as follows.

A. Surface elevation-motion modelling

The first model uses wave surface elevation as the model input and motions as the output. This input-output pair is written as surface elevation-motion for convenience. Although we have 7 cases of experimental data under different wave conditions (heights and period), we choose one of them to illustrate our modelling procedure and show the associated results. The case used here is $H_s = 0.06$m and $T_p = 1.0$s, with spectral peakedness $\gamma = 3.3$. For the full results for all the 7 cases are presented in the later part of this paper. The impact of different sampling rates, model orders and two different models (ARX and BJ) on the model performances (indicated by MSE and FPE, and 1, 3, 5 steps ahead prediction) is carefully investigated under repeatable modelling process. The data is separated into a training set and a testing set. The training set accounts for 70% of the data, while the testing set is 30%.

1) Comparison of sampling rate: When sampling the system, the Nyquist sampling condition $f_s \geq 2f_{max}$ needs to be satisfied, where f_{max} is the highest frequency of the signal and f_s is the sampling frequency. However, the best f_s is not fully known for M4 WEC system. The sampling rate is chosen as a prior based on engineer's experience and therefore it may not be optimal for modelling. Hence, we re-sample the data and investigate the impact of sampling rate on the model performances. The sampling rates are chosen as 32Hz, 16Hz, 8Hz and 4Hz. Moreover, the result of validation is under 1 step ahead of prediction. The results of the modelling are shown below.

From Table III, when the sampling rate reduces, the FPE and MSE of the model increase at the same time. The model performance becomes poorer for the larger FPE and MSE values. Meanwhile, the fit percentage of the testing data is decreasing. The reason for this phenomenon may be that the diminishing number of data results in inadequate samples. Therefore, the highest sampling rate for the modelling produces the best models, and it is selected in the following experiments.

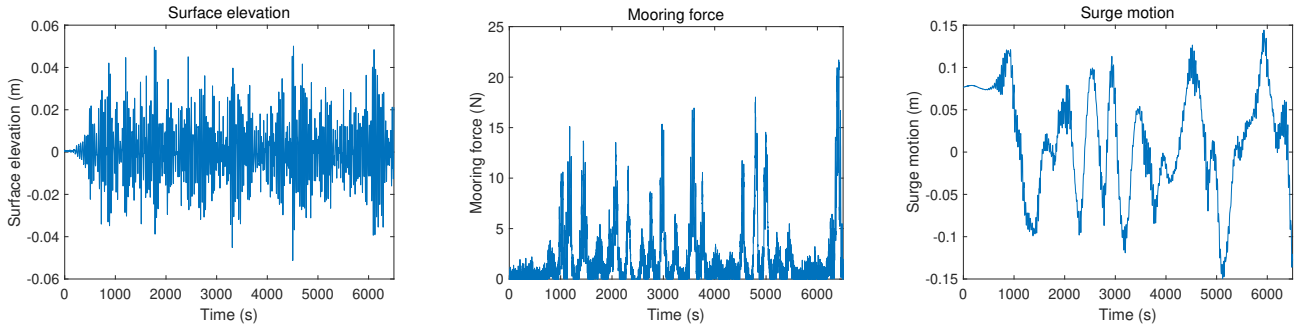

(a) (b) (c)

Fig. 5 Re-sampled measurements ($H_s = 0.06$m, $T_p = 1.0$s): (a) Surface elevation for wave excitation; (b) Mooring force; (c) Surge motion

TABLE III Comparison results of different sampling rates for ARX model

Sampling	Data	Training results			Testing results
		FPE ($\times 10^{-4}$)	MSE ($\times 10^{-4}$)	Fitting (%)	Fitting (%)
32Hz	19200	4972	4963	97.91	97.25
16Hz	9600	235.2	234.3	95.38	94.32
8Hz	4800	275.3	273.3	84.21	82.56
4Hz	2400	2.554	2.474	55.61	54.98

model order: [2 2 2]; $H_s = 0.06$m; $T_p = 1.0$s; elevation-motion

2) Comparison of model orders: Under sampling rate of 32Hz, different orders of ARX models are applied to the system identification. The orders considered here are [2 2 2], [4 2 1], [5 2 1], [10 2 1] and [15 16 20], respectively. Table IV presents the results of different orders of model. Some representative time-domain results from the trained model with order [2 2 2] are shown in Fig.6. As can be seen, the fitting percentage for the lowest model order [2 2 2] is 97.65%. When increasing the model order, the fitting percentage only improves marginally. A general principle in choosing a final model is that the simple model with lower order is often preferred if its performance is similar to the complex models with higher orders. In addition, the lower model order also enjoys fast computation speed. Therefore, the lower order [2 2 2] is chosen as the final model order.

For the same order of the model, different prediction horizons are applied to predict the output. In addition to the one step ahead prediction, the three and five step ahead predictions are also given. The multiple step ahead prediction can have larger accumulated errors and therefore the prediction errors increase with the length of steps. Results from different step ahead predictions are consistent. Only the lower orders and one step ahead prediction horizon are applied in the subsequent experiments.

3) Comparison of ARX and BJ models: In this section, the BJ model is applied to compare with the ARX model. In the experiment, the sampling time is still 32Hz and the prediction horizon is 1 step ahead. The training and validation of the BJ model are shown in Table V. It can be found that the lower order BJ models also perform similar to the higher order models, which holds the same conclusion with the results from ARX models. Hence, here the BJ model order is selected as [2 2 2 2 1].

In order to further validate the performance of ARX (or BJ) models, further experiments are conducted for 7 different wave conditions with different wave periods and heights (as shown in Table II) and Table VI shows the result of BJ model with order [2 2 2 2 1] as an example. The models perform well across 7 cases with a fitting percentage ranging from 94.84% to 99.57%. It is worth mentioning that the case ($T_p = 1.2$m, $H_s = 0.13$s) has the lowest fitting percentage of 94.84%.

B. Force-motion modelling

The second model uses top mooring force as the model input and motions (surge, pitch and heave) as the model output for system identification. This input-output pair is written as force-motion for simplicity. Also, both linear ARX and BJ models are used for comparative analysis under seven different wave condition cases and different sampling rates. As an example, Tables VII shows the results of modelling between top mooring force and surge motion under the first wave condition. It is worth noting that the fitting percentage of the lowest ARX model order [2 1 1] is 99.25%. The three and five-step prediction can also achieve a high fitting percentage. Therefore, ARX model order [2 1 1] is then selected for top force-surge motion modelling. Similar to ARX model, the lower order for BJ model also has satisfied performance and in this case the order [3 2 2 2 1] is selected.

Table VIII shows the different sampling time results of ARX and BJ modelling under the determined model orders. Similar to the results of the elevation-motion model, the values of MSE and FPE increase as the sampling rate reduces, which results in a poorer identification performance. The insufficient number of samples decreases the model fitting percentage. Hence, in this case, the highest sampling rate is selected for modelling.

TABLE IV Comparison of different ARX model orders

ARX order	Training results			Testing results Fitting (%)		
	FPE ($\times 10^{-7}$)	MSE ($\times 10^{-7}$)	Fitting (%)	1 step	3 step	5 step
[2 2 2]	6.317	6.311	97.65	97.04	89.19	78.00
[4 2 1]	5.147	5.139	97.65	97.19	89.98	79.08
[5 2 1]	4.972	4.963	97.91	97.25	90.02	79.36
[10 2 1]	4.600	4.584	97.99	97.29	90.37	80.36
[15 16 20]	4.490	4.465	98.02	97.32	90.60	80.99

$H_s = 0.06$m; $T_p = 1.0$s; elevation-motion

TABLE V Results of differnet BJ model orders

BJ order	Training results			Testing results Fitting (%)
	FPE ($\times 10^{-7}$)	MSE ($\times 10^{-7}$)	Fitting (%)	
[2 2 2 2 1]	5.227	5.271	97.85	97.21
[4 4 4 4 3]	4.524	4.513	98.01	97.32
[5 5 5 5 2]	4.291	4.278	98.06	97.40
[10 10 10 10 6]	3.801	3.766	98.18	97.47
[15 15 16 16 6]	3.620	3.586	98.22	97.50

$H_s = 0.06$m; $T_p = 1.0$s; elevation-motion

TABLE VI BJ modelling under 7 wave conditions

Wave structure		Training results			Testing results Fitting (%)
		FPE ($\times 10^{-8}$)	MSE ($\times 10^{-8}$)	Fitting (%)	
T_p=1.0	H_s=0.06	8.891	8.882	99.57	99.52
T_p=1.2		2.056	2.053	99.12	98.49
T_p=1.4		2.026	2.023	99.13	98.64
T_p=1.8		5.046	5.038	99.17	99.26
T_p=1.2	H_s=0.13	1.629	1.626	94.84	92.98
T_p=1.4	H_s=0.13	3.659	3.653	97.16	94.49
T_p=1.8	H_s=0.13	1.619	1.616	99.48	99.50

model order: [2 2 2 2 1], elevation-motion

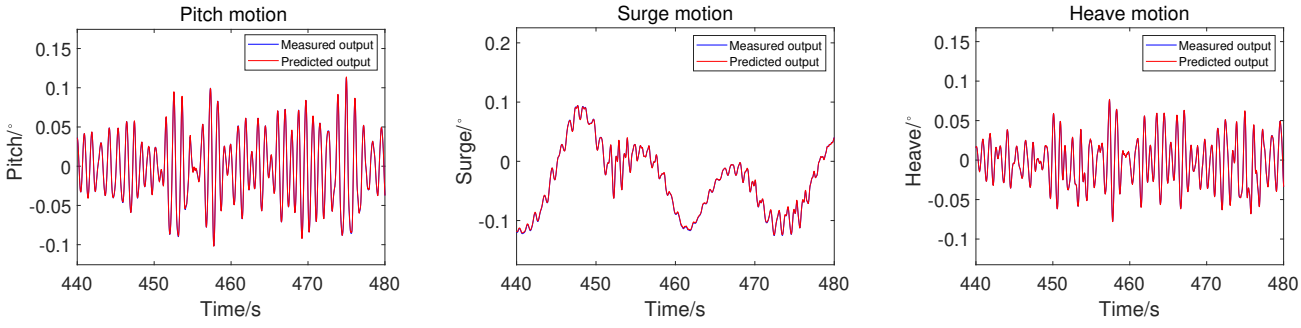

(a) (b) (c)

Fig. 6 One-step ahead trained model results of ARX model with order [2 2 2]: (a) pitch motion; (b) surge motion; (c) heave motion

TABLE VII Results of different ARX model orders

ARX order	Training results			Testing results Fitting (%)		
	FPE ($\times 10^{-8}$)	MSE ($\times 10^{-8}$)	Fitting (%)	1 step	3 step	5 step
[9 10 10]	6.822	6.789	99.63	99.56	97.51	93.53
[4 4 1]	7.882	7.866	99.60	99.52	97.28	93.16
[3 3 1]	8.905	8.892	99.57	99.52	97.19	92.86
[2 1 1]	27.26	27.23	99.25	99.11	95.20	89.22

$H_s = 0.06$m; $T_p = 1.0$s; top mooring force-surge motion

TABLE VIII Results of different sampling rates for ARX and BJ models

Data Length	ARX				BJ			
	Training results			Testing results	Training results			Testing results
	FPE ($\times 10^{-8}$)	MSE ($\times 10^{-8}$)	Fitting (%)	Fitting (%)	FPE ($\times 10^{-8}$)	MSE ($\times 10^{-8}$)	Fitting (%)	Fitting (%)
1200	3.536	3.490	72.92	67.92	1.041	1.020	85.36	84.43
2400	1.894	1.882	80.03	78.06	1.702	1.684	81.11	78.51
4800	4.261	4.249	90.51	90.81	2.566	2.555	92.64	92.49
9600	3.788	3.782	97.17	96.82	1.022	1.019	98.53	98.19
19200	2.726	2.723	99.25	99.11	8.914	8.902	99.57	99.52

$H_s = 0.06$m; $T_p = 1.0$s; top mooring force-surge motion; ARX model order: [2 1 1]; BJ model order: [3 2 2 2 1]

TABLE IX Results of different ARX model orders

ARX order	Training results			Testing results Fitting (%)		
	FPE ($\times 10^{-1}$)	MSE ($\times 10^{-1}$)	Fitting (%)	1 step	3 step	5 step
[2 2 1]	5.855	5.851	75.69	77.09	67.73	57.71
[4 3 1]	5.747	5.739	75.79	77.22	68.08	58.11
[5 5 1]	5.701	5.691	76.02	77.30	68.5	58.74
[10 6 1]	5.649	5.632	76.15	77.47	68.81	59.05
[20 18 13]	5.562	5.525	76.37	77.68	69.55	60.50

$H_s = 0.06$m; $T_p = 1.0$s; elevation-top mooring force

TABLE X Results of different BJ model orders

BJ order	Training results			Testing results
	FPE ($\times 10^{-1}$)	MSE ($\times 10^{-1}$)	Fitting (%)	Fitting (%)
[2 2 2 2 1]	5.641	5.636	76.14	77.46
[4 4 4 4 3]	5.540	5.531	76.36	77.69
[5 5 5 5 1]	5.536	5.523	76.38	77.63
[10 10 10 10 6]	5.532	5.511	76.40	77.70
[20 20 18 18 6]	5.350	5.303	76.85	78.04

$H_s = 0.06$m; $T_p = 1.0$s; elevation-top mooring force

C. Surface elevation-force modelling

The third model uses wave surface elevation as the model input and top mooring force as the output for system identification. Similarly, this input-output pair is written as elevation-force modelling for simplicity. The elevation-force models are essential to predict the minimised peak wave force given the measurements of the wave conditions, especially the periodic wave surface elevation information. Both ARX and BJ models are applied to test the model performances under seven wave condition cases. The sampling rate remains the same as previous two modelling cases.

Table IX shows the ARX modelling results. For different model order comparison, the conclusion is similar to the previous two modelling cases. The higher orders barely improves the fitting percentage while the lower order can also provide good performance. However, in this model, the fitting percentage is approximately 77% which is obviously lower than that in the previous two model cases. The modelling result of BJ models are shown in Table X. Similar to the performance of the ARX model, the BJ model also has approximately 76% fitting percentage. The results are slightly better than the ARX model with lower FPE and MSE, compared to the results of the ARX model in Table IX.

In this section we chose to focus on surge motion from the other two motions (heave and pitch) in our presented results because it has a particularly significant impact on the performance of the M4 WEC in practical applications. The heave and pitch motions, while certainly relevant and modeled, generally have less influence on the overall performance in this context.

V. Conclusion

In this paper, for the first time, two system identification methods, namely, autoregressive with exogenous inputs (ARX) and Box-Jenkins (BJ) models have been used to model the M4 wave energy converter (WEC) using wave surface elevation, top and bed mooring forces and the bow float motions including surge, pitch and heave under seven different wave condition cases based on the data collected via water basin experiments. The performance of models with different sampling rates and orders are also compared. Extensive results show that the lower order models have excellent fitting percentage and the model-system error is adequately small.

The findings from our study open several avenues for future investigations, promising to further expand our understanding of M4 WEC system. While our

present work focused on the system identification of M4 WEC, verifying wave conditions, surge motion response, and mooring force, however, the application of the method proposed in this paper is not restricted to these aspects.

1) Firstly, one of the key areas that we plan to explore is the application of our method to the investigation of the hydrodynamic characteristics of M4 WEC. This includes understanding how the device interacts with the dynamic forces of the water, which could provide deeper insights into its behavior under various wave conditions. Special attention will be given to the study of fluid-structure interaction, device motion, and wave diffraction and radiation effects.
2) Secondly, we aim to delve into the energy capture performance of the M4 WEC device. This will encompass the device's efficiency and effectiveness in harnessing wave energy, which is a critical factor determining its practical utility. We will scrutinize factors such as energy capture width and power take-off efficiency, which directly influence the energy conversion process.

Through these future research directions, we aspire to continue to contribute to the knowledge and technology development in the M4 WEC devices.

References

[1] K. Gunn and C. Stock-Williams, "Quantifying the global wave power resource," *Renewable Energy*, vol. 44, pp. 296–304, 2012.

[2] D. Lande-Sudall, J. Nyland, T. Rykkje, P. Stansby, and T. Impelluso, "Hydrodynamic modelling of a multi-body wave energy converter using the moving frame method," *Marine Structures*, vol. 87, p. 103332, 2023.

[3] D. Qiao, G. Zhi, H. Liang, D. Ning, J. Yan, and B. Li, "Scaling orchestration in physical model test of oscillating buoy wave energy converter," *Frontiers in Marine Science*, vol. 8, p. 627453, 2021.

[4] S. Gallagher, R. Tiron, E. Whelan, E. Gleeson, F. Dias, and R. McGrath, "The nearshore wind and wave energy potential of ireland: a high resolution assessment of availability and accessibility," *Renewable Energy*, vol. 88, pp. 494–516, 2016.

[5] A. Farkas, N. Degiuli, and I. Martić, "Assessment of offshore wave energy potential in the croatian part of the adriatic sea and comparison with wind energy potential," *Energies*, vol. 12, no. 12, p. 2357, 2019.

[6] S. Giorgi, J. Davidson, M. Jakobsen, M. Kramer, and J. V. Ringwood, "Identification of dynamic models for a wave energy converter from experimental data," *Ocean Engineering*, vol. 183, pp. 426–436, 2019.

[7] A. Elhanafi, G. Macfarlane, A. Fleming, and Z. Leong, "Experimental and numerical investigations on the hydrodynamic performance of a floating–moored oscillating water column wave energy converter," *Applied energy*, vol. 205, pp. 369–390, 2017.

[8] R. Ekström, B. Ekergård, and M. Leijon, "Electrical damping of linear generators for wave energy converters—a review," *Renewable and Sustainable Energy Reviews*, vol. 42, pp. 116–128, 2015.

[9] R. Ahamed, K. McKee, and I. Howard, "Advancements of wave energy converters based on power take off (pto) systems: A review," *Ocean Engineering*, vol. 204, p. 107248, 2020.

[10] H. Nguyen, C. Wang, Z. Tay, and V. Luong, "Wave energy converter and large floating platform integration: A review," *Ocean Engineering*, vol. 213, p. 107768, 2020.

[11] P. Stansby and E. C. Moreno, "Hydrodynamics of the multi-float wave energy converter m4 with slack moorings: Time domain linear diffraction-radiation modelling with mean force and experimental comparison," *Applied Ocean Research*, vol. 97, p. 102070, 2020.

[12] P. Stansby, S. Draycott, G. Li, C. Zhao, E. C. Moreno, A. Pillai, and L. Johanning, "Experimental study of mooring forces on the multi-float wec m4 in large waves with buoy and elastic cables," *Ocean Engineering*, vol. 266, p. 113049, 2022.

[13] P. Stansby, E. C. Moreno, and T. Stallard, "Large capacity multi-float configurations for the wave energy converter m4 using a time-domain linear diffraction model," *Applied Ocean Research*, vol. 68, pp. 53–64, 2017.

[14] R. A. Gonçalves, P. R. Teixeira, E. Didier, and F. R. Torres, "Numerical analysis of the influence of air compressibility effects on an oscillating water column wave energy converter chamber," *Renewable Energy*, vol. 153, pp. 1183–1193, 2020.

[15] L. Ljung, "System identification," *Signal Analysis and Prediction*, pp. 163–173, 1998.

[16] R. Ghanem and M. Shinozuka, "Structural-system identification. i: Theory," *Journal of Engineering Mechanics*, vol. 121, no. 2, pp. 255–264, 1995.

[17] W. Zhao, W. X. Zheng, and E.-W. Bai, "A recursive local linear estimator for identification of nonlinear arx systems: asymptotical convergence and applications," *IEEE Transactions on Automatic Control*, vol. 58, no. 12, pp. 3054–3069, 2013.

[18] H. Akaike, "Fitting autoregressive models for prediction," *Annals of the Institute of Statistical Mathematics*, vol. 21, no. 1, pp. 243–247, 1969.